# Inhibition of LILRB2 by a Novel Blocking Antibody Designed to Reprogram Immunosuppressive Macrophages to Drive T Cell Activation in Tumors

Ben Umiker*,[1], Yasmin Hashambhoy-Ramsay*,[1], Jeff Smith[1], Tanzila Rahman[1], Amy Mueller[1], Rachel Davidson[1], Christina Meyer[1], Gayatri Patankar[1], Mohammad Murshid Alam[1], Sarah Jaffe[1], Kristin Krukenberg[1], Allison Goodman[1], Vikki Spaulding[1], Michelle Priess[1], Abha Dhaneshwar[1], Masie Wong[1], Alexa Diiorio[1], Kristin O'Malley[1], Lara McGrath[1], Margaret Willer[1], Lauren Pepper[1], Monica Gostissa[1], Katalin Kis-Toth[1], Dmitri Wiederschain[1], Heather Cohen**,[1], Donald R. Shaffer**,[1]

***Co-first author**

****Co-last author**

**Affiliation: [1]Jounce Therapeutics, Inc., Cambridge, Massachusetts, United States of America**

**Corresponding Author: Ben Umiker,**
**Jounce Therapeutics**
**780 Memorial Drive, Cambridge MA 02139**
**Email: bumiker@jouncetx.com**

**Conflict of interest statement:** All authors were employees of Jounce Therapeutics during the time of study conduct

**Running Title:** Inhibition of LILRB2 Reprograms Tumor Macrophages

## ABSTRACT

Tumor-associated macrophages (TAMs) play an important role in maintaining the immunosuppressive state of the tumor microenvironment (TME). High levels of CD163+ TAMs specifically are associated with poor prognosis in many solid tumor types. Targeting TAMs may represent a key approach in development of the next generation of cancer immune therapeutics. Members of the leukocyte immunoglobulin-like receptor B (LILRB) family, including LILRB2 (ILT4), are known to transmit inhibitory signals in macrophages and other myeloid cells. Leveraging bulk and single cell RNAseq datasets, as well as extensive immunophenotyping of human tumors, we found that LILRB2 is highly expressed on CD163+ CD11b+ cells in the TME and that LILRB2 expression correlates with CD163 expression across many tumor types. To target LILRB2, we have developed JTX-8064, a highly potent and selective antagonistic monoclonal antibody. JTX-8064 blocks LILRB2 binding to its cognate ligands, including classical and non-classical MHC molecules. In vitro, JTX-8064 drives the polarization of human macrophages and dendritic cells toward an immunostimulatory phenotype. As a result, human macrophages treated with a LILRB2 blocker are reprogrammed to increase the activation of autologous T cells in co-culture systems. Furthermore, JTX-8064 significantly potentiates the activity of anti-PD-1 in allogeneic mixed lymphocyte reaction. In a human tumor explant culture, pharmacodynamic activity of JTX-8064 was observed in monotherapy and in combination with anti-PD-1. Collectively, our work provides strong translational and pre-clinical rationale to target LILRB2 in cancer.

## INTRODUCTION

Tumor-associated macrophages (TAMs) are tumor-resident innate immune cells often with an immunoinhibitory phenotype that are considered pro-tumorigenic[1]. Immunosuppressive macrophages are the most abundant CD163 expressing cells within the tumor microenvironment (TME). A high number of TAMs, characterized by CD163 expression, is an indicator of poor prognosis in clear cell renal cell carcinoma[2,3,4] ovarian cancer[5,6], head and neck squamous cell carcinoma[7,8] and other tumor types. Targeting the immunosuppressive macrophage population within the TME may lead to improved clinical outcomes for cancer patients. Identification of key checkpoint molecules that regulate macrophages that could be amenable to therapeutic intervention via blocking antibodies is in the forefront of current immuno-oncology (IO) efforts.

Leukocyte immunoglobulin-like receptor B2 (LILRB2), also referred to as immunoglobulin-like transcript 4 (ILT4), CD85d, or MIR10, is a cell surface receptor expressed on monocytes, macrophages, dendritic cells (DCs) and neutrophils. LILRB2 is generally not expressed on

lymphoid cells. LILRB2 binds endogenous ligands such as classical MHC-I[9] and non-classical MHC-I molecules, including HLA-G[10,11]. LILRB2 interfaces with the α3 domain of MHC-I molecules and the binding can occur in the absence of $\beta_2$-microglobulin ($\beta_2$m) on MHC-I, while closely related family member LILRB1 associates with MHC-I in $\beta_2$m-dependent manner[12].

The immunosuppressive nature of LILRB2 signaling through the binding of MHC-I has been described in multiple settings. HLA-G plays a key role at the fetal-maternal interface in tolerizing the mother's immune system to the developing fetus[13]. Soluble HLA-G binding to LILRB2 inhibits DC function, leading to suboptimal antigen presentation and a diminished CD4+ and CD8+ T cell response. Silencing LILRB2 using small interfering ribonucleic acid (siRNA) reverses HLA-G-induced immunosuppression of DCs and restores T cell proliferation[14]. LILRB2 binding to HLA-B is positively associated with human immunodeficiency virus (HIV)-1 replication across a large cohort of subjects. HLA-B haplotypes with the highest affinity binding to LILRB2 modify antigen-presenting properties of DCs leading to higher HIV-1 viral loads in patients[15]. Similarly, tumors employ a variety of strategies to evade detection and targeting by the immune system. HLA-G is upregulated in a significant number of malignant tissues as an immune escape strategy[16]. Thus, we and others hypothesized that the interaction between MHC-I molecules and LILRB2 expressed on macrophages, DCs and monocytes represents a myeloid based immune checkpoint in the TME. Chen et al. demonstrated the immunosuppressive role for LILRB2 in cancer, using antibodies specific for LILRB2. These anti-LILRB2 ligand blocking antibodies alter the maturation of macrophages within the TME to promote anti-tumor immunity[17].

Encouraged by these results, we have developed JTX-8064, a highly potent and specific blocker of LILRB2 for therapeutic applications in immuno-oncology. JTX-8064 is a humanized monoclonal antibody (mAb), consisting of 2 hinge-stabilized immunoglobulin gamma 4 (IgG4, with the S228P mutation) heavy chains and 2 immunoglobulin kappa (Igκ) light chains. JTX-8064 binds to human LILRB2 with high specificity and blocks the interaction of LILRB2 with MHC-I molecules, thereby reprogramming macrophages from an immunosuppressive to an immunostimulatory phenotype. Human monocyte-derived macrophages (HMDMs) were used to assess the activity of JTX-8064. JTX-8064 treatment potentiated lipopolysaccharide (LPS)-induced TNFα, while potently suppressing IL-10 production in HMDMs. In the absence of LPS stimulation, exposure of HMDMs to JTX-8064 shifted the profile of the macrophages towards an immunostimulatory state. Furthermore, HMDMs differentiated in the presence of JTX-8064 were able to stimulate T cells to produce IFNγ and proliferate in both autologous and allogenic co-culture systems. Finally, in a more complex *ex vivo* human tumor histoculture system, JTX-8064 re-programmed TAMs and indirectly activated T cells in a subset of tumor samples. Collectively, these data demonstrate that JTX-8064 treatment converts immunosuppressive macrophages toward a more immune stimulatory state and thus contributes to an effective T cell response.

## MATERIALS AND METHODS

### Generation of JTX-8064 and chimeric pre-cursor RCM-15

The parent antibody of JTX-8064, RCM15, was obtained from an antibody discovery campaign performed at Antibody Solutions and screened at Jounce from Brown Norway rats immunized with hLILRB2-His (the human ECD of LILRB2 with a 6x histidine tag). The RCM15 mAb was identified from a rat hybridoma library and was selected based on its ability to specifically bind human LILRB2 with no binding to the other 10 LILR family members. It was also selected for the ability to block binding of HLA-G, along with other classical HLA family members.

Humanization designs of RCM15 were generated at Fusion Antibodies LLC. CDRs were identified using numbering systems from IMGT and Kabat combined. Online databases of human IgG sequences were searched to compare to the rat VH and VL domains using the BLAST algorithm. These search results were refined through analysis of framework homology, maintenance of key framework residues and canonical loop structure to a top set of four mature human IgG sequences and a fifth closest human germline sequence. CDRs were grafted into these five selected frameworks and back mutations to the rat germline were selected to maintain residues at the VH/VL interface and in the canonical loop structure. The humanized variants were checked to determine whether they had been humanized in accordance with WHO's definition of humanized antibodies.

The selected lead candidate, JTX-8064, was constructed with the variable regions of the humanized RCM15 variant and the human IgG4 isotype backbone containing a mutation at amino acid residue 228 (S228P). The sequence the Heavy and light chain of JTX-8064 can be found in the following document is found in Supplemental Figure 1

### *In vitro* macrophage and dendritic cell assays

*Generation of human monocyte-derived macrophages and DCs***.** Whole blood or buffy coats from healthy donors were obtained from Research Blood Components. PBMCs were isolated by Ficoll-Hypaque density gradient. CD14+ monocytes were purified using negative magnetic selection (EasySep™ Human Monocyte Isolation Kit, STEMCELL Technologies). Alternatively, human pre-purified frozen monocytes were obtained (STEMCELL Technologies). Monocytes were cultured for 6-8 days in differentiation media (RPMI (ThermoFisher) and 10% HI-FBS (Millipore Sigma) with 40 ng/mL M-CSF (BioLegend) for macrophages (HMDM); or 40 ng/mL each IL-4 and GM-CSF (BioLegend) for DCs (HMDDC). On day 2 or 3 media was refreshed by adding FBS containing media with necessary cytokines (e.g. GM-CSF/IL-4 or M-CSF) to the cultures. For experiments where anti-LILRB2 and isotype antibodies were included throughout differentiation, antibodies were added to the differentiation media at a concentration of 1 µg/mL.

*HLA-A2 and HLA-G tetramer blocking.* HMDMs or CHO-S LILRB2-overexpressing cells were incubated with different concentrations of anti-LILRB2 or isotype control antibodies for 30 min. After incubation, cells were washed and subsequently incubated with 5 µg/mL of APC-conjugated HLA-A2 or HLA-G tetramer (Fred Hutch Immune Monitoring Core) for 30 min. Cells were washed again and then analyzed by flow cytometry. Percent tetramer blocked was calculated by the formula: 100% - [(tetramer + antibody)/(tetramer alone)] where values are in geomean mean fluorescence intensity (MFI).

*Macrophage cytokine release.* HMDMs were stimulated with 100ng/mL LPS-EB (Invivogen) and treated with different concentrations of anti-LILRB2 or isotype control antibodies for 24h. Supernatants were collected and analyzed by multiplex Cytometric Bead Array (BD Biosciences) according to manufacturer's instructions for TNFα and IL-10 on a BD Celesta flow cytometer.

*Macrophage and DC differentiation in the presence of anti-LILRB2.* HMDMs and HMDDCs differentiated in the presence of anti-LILRB2 or isotype antibodies were harvested on day 7 of differentiation. Cells were first stained with LIVE/DEAD™ Fixable Near-IR Dead Cell Stain Kit (ThermoFisher) for 30 min at 4°C. Cells were then blocked with Human Fc-Block and True-Stain Monocyte Blocker (BioLegend) for 30 min at 4°C to prevent non-specific staining of flow antibodies before staining cells for 30 min at 4°C. The antibodies used for staining included CD163-BUV395 (clone GHI/61) from BD Biosciences, and CD86-PE (clone IT2.2), DC-SIGN-BV421 (clone 9E9A8) from BioLegend. Cells were fixed with 2% paraformaldehyde before being run on a BD Fortessa flow cytometer. In separate experiments, cells were blocked with Human Fc-Block followed by staining with CD163-FITC (clone GH1/61) and CD14-BV605 (clone M5E2) antibodies from BioLegend.

*Gene expression analysis.* Monocytes from healthy donors were treated for 24h with either JTX-8064 or a control IgG4 antibody, and a baseline sample was taken before treatment was administered. Gene expression profiling was performed by NanoString nCounter® using the Human Immunology V2 panel with a custom macrophage-specific spike-in. Raw data was normalized to housekeeping genes, log2 transformed, and then adjusted for noise based on a negative control threshold for downstream analysis.

**PBMC allogeneic reaction**

Frozen primary human PBMCs (STEMCELL Technologies) were thawed for 2 min in a water bath at 37°C. Cells were added dropwise to warm complete culture medium and counted using an automated cell counter (Vi-CELL XR Cell Viability Analyzer, Beckman Coulter). Cells were spun down at 400G for 5 min and resuspended in warm complete culture medium at $1x10^6$ cells/mL. PBMCs from two donors were incubated together with 10 µg/mL of varying monotherapy or combination therapy antibody treatments in a total volume of 200 µL in 96-well round-bottomed plates. $5x10^4$ cells/well were plated for each donor for a total of $1x10^5$ cells/well. Supernatants were harvested after a 5-day incubation.

IFNγ was measured in experimental supernatants using a bead-based immunoassay, a Cytometric Bead Array (CBA) Human IFNγ Flex Set (BD Biosciences), according to the manufacturer's instructions.

**Macrophage and T cell autologous co-culture**

PBMCs were counted, 2/3 of the PBMCs were resuspended in Bambanker™ cell freezing medium and kept frozen for 7 days until T cell isolation. CD14+ monocytes were isolated from the remaining PBMCs by negative magnetic separation using STEMCELL EasySep Human Monocyte Isolation Kit according to the manufacturer's protocol. Isolated monocytes were counted and adjusted to a concentration of $1x10^6$ cells/mL in macrophage differentiation media (RPMI+10% FBS+40 ng/mL rhM-CSF). Antibodies were prepared as a 2x solution in macrophage differentiation media. 150 mm tissue culture-treated petri dishes were prepared with 5 mL of isolated monocyte suspension and 5 mL macrophage differentiation media containing antibody was added to designated plates. All plates were incubated at 37°C for 7 days. On day 4, 5 mL of macrophage differentiation media containing antibody was added to designated plates. On day 7 media was aspirated from plates and 10 mL cold PBS+5 mM EDTA was added. Cells were then washed, counted and adjusted to desired concentration in RPMI + 10% FBS. On day 7 autologous PBMCs were thawed and CD3+ T cells were isolated from previously frozen PBMCs by magnetic separation using the EasySep Negative selection kit and adjusted to a concentration of $2x10^6$ cells/mL in assay medium (RPMI+10% FBS). $1x10^5$–$3.2x10^6$ T cells/100 µL were added designated wells of a 96-well clear, round-bottom tissue culture-treated plate pre-coated with 1 mg/mL anti--human CD3 antibody (clone OKT3). $1x10^5$ HMDMs/100 mL were added to designated wells and incubated at 37°C for 3 days. After incubation, plates were centrifuged at 400g for 3 min to pellet the cells and cell culture supernatants were collected. T cell number was determined by staining the cells with anti-CD3-PE antibody. Secretion of IFNγ was measured in the cell culture supernatant via cytokine bead array (CBA).

**Macrophage and T cell allogenic mixed lymphocyte reaction (MLR)**

Monocytes were cultured in M-CSF containing media for 7 days to obtain macrophages. Frozen T cells were thawed, combined at 1:5 macrophage to T cell ratio and treated with antibodies at 1 µg/mL for 5 days. Secreted cytokines were measured from collected supernatants by CBA.

**JTX-8064 binding to peripheral monocytes and neutrophils**

Fresh human blood (Research Blood Components) from two donors was lysed with ACK lysis buffer for 15 min on ice. Cells were first stained with LIVE/DEAD™ Fixable Near-IR Dead Cell Stain Kit (ThermoFisher) for 30 min at 4°C. Cells were then blocked with Human Fc-Block (Biolegend) for 30 min at 4°C to prevent non-specific staining of flow antibodies before staining cells for 30 min at 4°C. The antibodies used for staining included CD14-BV421 (clone M5E2), CD177-FITC (clone MEM-166) and HLADR-BV510 (clone G46-6) from Biolegend. Cells were stained in a 96-well plate with this cocktail as well as a 3-fold 11-point titration of unlabeled JTX-8064 or IgG4 control antibody starting at a concentration of 66.67 nM. Cells were washed

and then incubated with anti-hIgG4-biotin (Mabtech) for 30 min at 4°C, before being stained with Streptavidin-APC (Biolegend) for 30 min at 4°C and run on a BD Fortessa flow cytometer.

**Flow cytometry-based profiling of PBMCs and tumor-infiltrating lymphocytes (TILs)**

*LILRB2 expression on peripheral monocyte subsets.* Healthy donor PBMCs were obtained frozen from STEMCELL Technologies or isolated from buffy coats from Research Blood Components. Cancer patient PBMCs were obtained from Discovery Life Sciences. Cells were first stained with LIVE/DEAD™ Fixable Near-IR Dead Cell Stain Kit (ThermoFisher) for 30 min at 4°C. Cells were then blocked with Human Fc-Block and True-Stain Monocyte Blocker (BioLegend) for 30 min at 4°C to prevent non-specific staining of flow antibodies before staining cells for 30 min at 4°C. The antibodies used for staining included CD3-FITC (clone HIT3A), CD56-FITC (clone 2H7), CD20-FITC (clone MEM-188), CD16-BV510 (clone 3G8), LILRB2-APC (clone 42D1) from BioLegend; CD45-BUV805 (clone HI30), CD14-BUV737 (clone M5E2) from BD Biosciences; CD19-PE (clone HIB19), CD3-BV421 (clone UCHT1), CD14-BV785 (clone M5E2), CD177-FITC (clone MEM-166) from BioLegend; LILRB2-Dylight-650 (clone RCM15.006) was produced at Jounce. For each PBMC sample, cells were also stained with isotype panel where LILRB2 antibodies are replaced with isotype controls. Cells were fixed with 2% paraformaldehyde before being run on a BD Fortessa flow cytometer. To calculate antibody binding capacity for the anti-LILRB2 flow cytometry antibody, Quantum™ Simply Cellular® Beads (Bangs Laboratories) were used according to manufacturer's instructions.

*Tumor infiltrating lymphocyte analysis.* To assess LIRB2 on TILs, tumor samples were acquired from patients with lung, renal or uterine cancer. Tumors procured from hospitals associated with Cooperative Human Tissue Network (CHTN) were dissociated using Tumor Dissociation Kit, Human from Miltenyi Biotec following the manufacturer's instructions. Dissociated cells were frozen down in Bambanker medium until use for flow cytometry. To prepare samples for flow cytometry, samples were first stained with LIVE/DEAD™ Fixable Near-IR Dead Cell Stain Kit from ThermoFisher Scientific diluted 1:2000 in PBS for 30 min in the dark on ice. Cells were then centrifuged and washed in FACS buffer (Dulbecco's phosphate buffered saline (dPBS)+2% FBS+0.2mM EDTA). The samples were blocked with Human TruStain FcX™ block, mouse IgG2b and monocyte blocker all at a 1:20 dilution in FACS buffer for 20 min. After the blocking step, granulocytes were incubated with fluorescently conjugated antibodies (anti-CD45 (BUV805), anti-CD3 (FITC), anti-CD11b (BV605), anti-CD163 (BV711), anti-LILRB2 (APC), LILRB2 isotype control (APC) diluted in FACS buffer for 30 min on ice protected from light. Fluorescence minus one controls (FMOs) were performed for CD163 and LILRB2 for gating. Samples were washed twice with FACS buffer and fixed in 4% paraformaldehyde, then acquired on a BD Fortessa flow cytometer and data was analyzed with FlowJo™.

***Ex vivo* tumor histocultures**

Fresh human treatment-naïve tumor samples were obtained post-surgery from kidney, lung and head and neck cancer patients. A section of each tumor was manually cut, formalin-fixed

and paraffin-embedded for IHC analysis. The remaining tumor was manually cut into slices. The tissues were sectioned with the following instrument settings; thickness: 300 mM, speed: 2, and frequency: 9. Frequency and speed settings may need to be adjusted for varying tumor textures. Commonly used speed range is 2-5. Commonly used frequency range is 6-9. Higher frequencies are used for softer tumors. One slice was stored in RNAlater at 4°C, and the remaining slices were transferred to a polycarbon membrane inserted in 6-well plate containing assay media (1:1 AIM-V/RPMI, 10% human serum, 100u/mL Penicillin Streptomycin, 2 mM Glutamax, 0.055 mM 2-mercaptoethanol, 0.01 M HEPES, 1X MEM non-essential amino acids, 1 mM sodium pyruvate, 1x insulin-transferrin-selenium, 0.5 g/mL fungizone) within the outer well and were fully submerged in the media. JTX-8064 and/or pembrolizumab (anti-PD-1 antibody) treatments were immediately added into the media and plates were incubated at 37°C. Each slice was treated with 10 µg/mL of drug for 24h; in instances where samples were treated with more than one drug, 10 µg/mL of each drug was used. After incubation, tumor slices were removed from media and stored in RNAlater at 4°C.

**RNA processing and gene signature analysis**

*Sample processing.* RNA was extracted using the Promega Maxwell® RSC Simply Cells RNA kit. Extracted RNA was then processed on the Agilent TapeStation using the RNA Screentape to determine the quality and quantity of RNA present. 50 ng of RNA was then processed on the NanoString platform using the Immunology V2 base codeset and a custom designed spike-in.

*Calculating gene expression signature scores.* The M1 and M2 signatures are composed of the membrane receptors, cytokines and chemokine genes identified by Martinez et al[18] that were measured using NanoString. The IFNγ signature is composed of genes that displayed modulated expression in response to anti-PD-1 treatment in histoculture. The tumor associated macrophage cell signature (TAM signature) was defined based on genes that correlate with known macrophage cell markers. Signature scores were calculated for each sample by averaging the normalized expression of component genes and the component genes can be found in Supplemental Figure 2. The macrophage polarization signature score is calculated by subtracting the M2 signature score from the M1 signature score.

*Normalization and setting noise thresholds.* Data from anti-LILRB2, anti-PD-1 or anti-LILRB2+anti-PD-1 treated samples was normalized to the average of matched IgG4 anti-RSV negative control treated samples from the same donor. Noise in the histoculture system was evaluated by examining gene expression from tumor samples that had at least two slices treated with the control antibody. A total of 153 histoculture slices from 70 tumor samples, including kidney, lung and head and neck, were analyzed to determine noise thresholds. The expression of each gene from each anti-RSV treated sample was normalized to average expression of that gene across anti-RSV treated samples from the same tumor, and then pharmacodynamic (PD) gene signatures were calculated. The noise threshold for each PD gene

signature was defined as the 95$^{th}$ percentile of the distribution of the signature scores across the 153 samples and PD responders were identified as tumors with an average treatment-induced PD signature score greater than the noise threshold for that signature.

LILRB2 surrogate signature: NanoString probe specificity experiments have shown that the LILRB2 probe is non-specific and binds to other LILR- family members, which prompted development of a LILRB2 surrogate signature. NanoString analysis on 124 baseline Histoculture samples with matching LILRB2 qPCR analysis was used to generate the signature. The spearman correlation coefficient was calculated between each NanoString gene and LILRB2 qPCR values, and the top 25 genes with the highest correlation were investigated further. Highly correlated genes that overlapped with existing macrophage cell type and tumor associated macrophage signatures were selected to be part of the surrogate signature. A signature score was calculated with this subset of genes and showed a 0.73 spearman correlation coefficient to LILRB2 qPCR. Additionally, this surrogate signature was separately tested in TCGA bulk RNA for lung cancer indications and shows a high correlation of 0.91 to LILRB2. LILRB2 NanoString surrogate signature: FCER1G, SPI1, CYBB, LILRB1, CD86, C1QA, C1QB

**Control human IgG4 antibody**

In all experiments the control IgG4 antibody is a Jounce-produced control anti-RSV antibody based on the palivizumab sequence on a human IgG4 backbone.

**Quantitative polymerase chain reaction analysis of LILRB2**

A LILRB2-specific gene expression assay was developed utilizing quantitative polymerase chain reaction (qPCR) and probe-based detection via Applied Biosystems TaqMan™ detection chemistry. The housekeeping gene glyceraldehyde 3-phosphate dehydrogenase (GAPDH) was used in conjunction with the LILRB2 assay to allow for data normalization and to provide an internal control for the polymerase chain reaction (PCR). RNA (200ng) was subjected to a reverse transcription reaction where first strand cDNA was synthesized using the Bio-Rad Laboratories iScript™ Reverse Transcription Supermix from reverse transcription quantitative polymerase chain reaction (RT-qPCR) kit, according to the manufacturer's published protocol. The resulting cDNA was subjected to qPCR. The TaqMan™ Fast Advanced Master Mix was used in conjunction with the TaqMan™ assay for GAPDH (Hs02786624_g1) with VIC dye label and the LILRB2 assay, which was ordered from IDT as a PrimeTime qPCR assay, with FAM dye label. Assays were set up in triplicates. PCR plates were loaded into the Applied Biosystems QuantStudio™ 7 and run using the standard TaqMan™ cycling profile with the anneal temperature at 65°C. Data was analyzed using the QuantStudio real-time PCR software. The efficiencies for the assays were calculated for each run to account for plate-to-plate variability.

**Single cell RNA sequencing data processing**

Single-cell RNAseq raw counts or TPM matrices and cell-level metadata were downloaded from the data repositories referenced in the original papers.[19,20,21] Datasets were processed in R

version 3.6.3 and Seurat v3.2.0 using a general Seurat workflow with the following functions: CreateSeuratObject, NormalizeData, FindVariableFeatures, ScaleData, RunPCA, FindNeighbors, FindClusters, RunUMAP. Cell type annotations were based on original authors' labels if available or based on enrichment of expression of cell type specific marker genes in each cluster. Clustered cells were visualized in low dimensional space defined by the UMAP components, UMAP1 and UMAP2, with cell type labels annotated using DimPlot and the gene expression of LILRB2 and TAM signature score annotated using FeaturePlot. The TAM signature score denotes the mean expression of log normalized gene expression of genes in the signature in each cell.

**Surface plasmon resonance mAb affinity analysis**

Affinity assessment was performed to measure binding characteristics of JTX-8064 to recombinant Human LILRB2 ECD His-tag fusion protein using surface plasmon resonance (SPR) (Sierra SPR-32, Bruker Corporation). A high-capacity amine chip was pre-immobilized with AffiniPure goat anti-human IgG, Fcγ fragment-specific antibody. JTX-8064 was captured on the anti-human Fc surface at 2 µg/mL in SPR running buffer (PBS+0.02% Tween20) for 30 sec. Control IgG4 was also captured at 2 µg/mL for 30 sec and used as a negative control reference surface. Human LILRB2 ECD His-tag was flowed over the JTX-8064 and reference surface in 7 serial dilutions of 2.5-fold starting 60 nM for 300 sec at a flow rate of 10 µL/minute, followed by buffer injection for 900 sec at 10 µL/minute. JTX-8064 and LILRB2 ECD His-tag was then removed with 2 20 sec injections of 10 mM Glycine, pH 2.0 and the experiment was repeated 4 times. The data was analyzed using the Sierra Analyzer software (version 3.1.34). Buffer only condition and negative control reference surface were subtracted from JTX-8064 curves and fitted to a 1:1 Langmuir Fit.

**Neutrophil Activation Assay**

Human blood was treated with dextran (6 mg/mL), DCFDA (125 µM) and treatment antibodies in a dose titration manner in a 37$^{o}$C water bath for 20 min. After incubation, 300-500 µl of leukocyte-rich plasma from each sample was transferred to a new 1 mL clear polypropylene tube and was incubated in 37$^{o}$C water bath for 10 min. 50 µl of leukocyte-rich plasma suspensions from each tube was transferred to a well of a 96-well round bottom tissue culture treated plate placed on ice for subsequent labeling of cells. The following antibodies were diluted 1:50 in FACS buffer containing Fc Block (1:20) and used for labeling: anti-CD11b PE, anti-CD62L APC, anti-CD14 PECy7, antiCD16 BV421. The samples were analyzed by flow cytometry.

**Data Availability**

The data generated in this study are available upon request from the corresponding author, publicly available data generated by others were used by the authors in the case of single cell RNA sequencing data.

## RESULTS

### LILRB2 expression is confined to myeloid cells in the tumor microenvironment with high expression on CD163+ CD11b+ cells

To assess LILRB2 expression in the TME at the single-cell level, we analyzed over 400,000 single cell transcriptomes from 143 patients across 7 cancer types[19,20,21,22,23,24,25]. LILRB2 mRNA and the TAM signature were specific to myeloid cell clusters in the TME compared to other cell types (e.g., T cells, NK cells) in head and neck cancer patients (Fig. 1A), melanoma patients (Fig. 1B) and in a mix of colorectal, lung, breast and ovarian cancer patients (Fig. 1C). Throughout all data sets LILRB2 and the TAM signature clustered together. We also found examples of smaller clusters showing lower expression of LILRB2 but with significant expression of the TAM signature. Similarly, there are clusters of cells that express the LILRB2 and are TAM signature negative. The expression of LILRB2 has been observed on dendritic cells, plasmacytoid DCs, monocytes and other myeloid subsets within the tumor microenvironment and periphery. These cells express varying levels of the TAM signature; therefore, it is likely that there are myeloid cells that are LILRB2 positive but not strongly positive for the TAM signature.

CD163 is expressed on immunosuppressive macrophages in the tumor[26]. Thus, we examined whether LILRB2 is expressed at high levels on CD163+ CD11b+ cells. Flow cytometry analysis of 3 different tumor types (NSCLC, renal and uterine) showed significantly higher expression of LILRB2 on CD163+ CD11b+ cells as compared to CD163- CD11b+ cells (Fig. 2A) Conversely, the average expression of CD163 was significantly higher on LILRB2+ CD11b+ cells when compared to LILRB2- CD11b+ cells (Fig. 2B). Expression of CD163 by immunohistochemistry (IHC) was observed across tumor types, including primary and metastatic tumors (Fig. 2C), suggesting that the same may be the case for LILRB2. However, specific assessment of LILRB2 protein expression by immunohistochemistry (IHC) is problematic because of the high structural similarities between LILRB family members.

To expand our analysis of LILRB2 and CD163 expression to a larger subset of tumor samples, we examined their RNA levels across multiple tumor types. Across all samples analyzed from The Cancer Genome Atlas (TCGA), a strong correlation was observed between LILRB2 and CD163 expression specifically on TAMs (Fig. 2D). Based on these observations, we concluded that CD163 can be considered as a surrogate marker for LILRB2 expression to identify TAMs, since no suitable anti-LILRB2 antibody has been identified for IHC, including JTX-8064 which does not bind to LILRB2 in fixed tissue.

### LILRB2 is highly expressed on circulating monocytes in healthy donor and cancer patient blood

We investigated LILRB2 receptor number on peripheral leukocytes from healthy donors and cancer patients, as well as on tumor infiltrating lymphocytes (TILs) from a variety of solid tumors (clear cell Renal Carcinoma, Non-small Cell Lung Carcinoma, Head and Neck Squamous

Cell Carcinoma (Supplementary Fig. 3). The average number of LILRB2 receptors per cell for monocytes, neutrophils, B cells and T cells was measured. LILRB2 expression was found to be highest on peripheral monocytes, with significant expression also observed on neutrophils in healthy donor PMBCs (Supplementary Fig. 4A). No significant difference in LILRB2 expression was observed on monocytes between matched PBMC and dissociated tumor-resident cells from cancer patients of the 3 tumor types tested (Supplementary Fig. 4B).

Expression of LILRB2 was also assessed on monocyte subsets from both healthy peripheral blood samples and blood samples from cancer patients diagnosed with head and neck, ovarian, NSCLC, and renal cancers. Data are shown as aggregate for different tumor types. 100% of classical monocytes (CD14+, CD16-) and 100% of intermediate monocytes (CD16++, CD14+) expressed LILRB2 (Supplementary Fig. 4C). However, in healthy donor and cancer patient blood there was variation in the number of non-classical (CD16++, CD14-) monocytes that express LILRB2 (Supplementary Fig. 4C). LILRB2 expression was significantly higher on intermediate monocytes than on classical or non-classical, though no significant differences in LILRB2 levels were noted on monocyte subsets between healthy donors and cancer patients (Supplementary Fig. 4D). Gating strategy to define monocyte subsets is found in Supplemental Figure 5. Collectively, our data indicate that LILRB2 expression is primarily confined to monocytic cells and neutrophils in the peripheral blood, with no appreciable differences between healthy donors and cancer patients. Furthermore, LILRB2 levels appear to be the highest on intermediate monocytes versus other subsets, with a lower proportion of non-classical monocytes expressing LILRB2.

**JTX-8064 is a monoclonal antibody that specifically binds to LILRB2 and blocks HLA ligand binding**

To target LILRB2-mediated immune suppression, we set out to generate a highly specific anti-LILRB2 antibody with strong potential to inhibit ligand binding. JTX-8064 was constructed with humanized variable regions fused to the human IgG4 backbone containing a hinge-stabilizing mutation (S228P). JTX-8064 specifically bound LILRB2 and had no detectable binding to the other 10 closely related LILR family members expressed on CHO-S cells (Fig. 3A). The positive control cross-reactive polyclonal antibody showed detectable binding to all relevant LILR family members on the CHO-S cells.

Surface plasma resonance (SPR) data revealed that JTX-8064 bound with high affinity to a purified LILRB2 protein. The Kd value was 3.18+/-0.083 nM with an association rate constant of 6.58x105 M-1s-1, and a dissociation rate constant of 2.09x10-3 s-1 (Fig. 3B). Binding of JTX-8064 was observed in a dose dependent manner on both neutrophils and monocytes from whole blood samples (Fig. 3C).

Soluble JTX-8064 and control human IgG4 antibody were tested for the ability to disrupt HLA-G or HLA-A2 binding to LILRB2 on HMDMs. JTX-8064 potently blocked HLA-G and HLA-A2 binding to HMDMs in a dose-dependent manner (Fig. 3D and 3E). JTX-8064 blocked HLA-A2 tetramer at maximum of ~50% and HLA-G tetramer at a maximum of ~40% on HMDMs. However, nearly complete blocking of HLA-G was observed when CHO-S cells overexpressing LILRB2 were used, demonstrating that JTX-8064 is capable of completely blocking LILRB2 binding to HLA-G in this system (Fig. 3F).

These findings demonstrate that JTX-8064 is a potent blocker of LILRB2 ligand binding and imply that LILRB2 is not the sole receptor for HLA-G and HLA-A2 on HMDMs.

**JTX-8064 enhances pro-inflammatory activation of macrophages and downregulates key immunoinhibitory signaling leading to increased allogenic T cell activation in pre-clinical studies**

To investigate the biological effects of our anti-LILRB2 antibody, soluble JTX-8064 and IgG4 control antibody were tested on LPS-treated HMDMs (at concentrations ranging from 66 nM-6.6x10$^{-}$5 nM) by 10-fold serial dilutions. JTX-8064 increased LPS-induced production of TNFα and inhibited production of immunosuppressive cytokine IL-10 in a dose-dependent manner (Fig. 4A and 4B). The EC50 concentration for TNFα production was 0.01356 nM and the IC50 concentration for IL-10 production was 0.01425 nM.

A pre-humanized variant of JTX-8064 and negative control human IgG4 antibody were also tested on HMDMs at a single concentration of 10 µg/mL to study gene expression changes. Anti-LILRB2 antibody treatment induced significant transcriptome modulation, including upregulation of genes associated with pro-inflammatory M1 macrophages and downregulation of genes associated with M2/immunosuppressive macrophages using previously described analysis methodology[24] (Fig. 4C and 4D). In the same experiments, anti-LILRB2 antibodies significantly downregulated CD163 and CD14 protein expression on macrophages (Fig. 4E and 4F). Signaling via phosphorylation of STAT3 (pSTAT3) has been shown to induce an M2 functional state in macrophages[25]. Anti-LILRB2 inhibited the accumulation of pSTAT3 in HMDMs after LPS stimulation for 24h (Fig. 4G). Lastly, JTX-8064 potentiated anti-PD-1 response in the activation of T cells in macrophage/CD3+ T cell mixed lymphocyte reactions. The combination of JTX-8064 and anti-PD-1 increased the level of IFNγ over anti-PD-1 in MLR cultures (Fig. 4H). Antagonizing LILRB2, however, did not activate neutrophils as measured by CD11b high frequency on cultured neutrophils (in this assay alemtuzumab, a potent CD52 binding antibody, was used as positive control) (Supplementary Fig. 6).

Taken together, our data show that our anti-LILRB2 antibodies reverse an immunosuppressive phenotype of human monocyte derived macrophages and promote a more immunostimulatory

phenotype in these cells. The chimeric antibody, RCM15 was humanized in the development of JTX-8064 was selected for its favorable characteristics compared with other anti-LILRB2 chimeric antibodies tested for HLA-G blocking and TNF alpha secretion in a macrophage activation assay (Supplemental Fig. 7).



**JTX-8064 drives monocyte differentiation to macrophages and DCs cells that potently activate T-cells in co-culture**

To investigate the effects of LILRB2 blocking on monocyte differentiation to macrophages, HMDMs were differentiated from monocytes in the presence of 1 μg/mL soluble JTX-8064 or negative control human IgG4 antibody. Following differentiation, the HMDMs were co-cultured with autologous T cells in the presence of a plate bound anti-CD3 antibody. Macrophages generated in the presence of JTX-8064 enhanced IFNγ secretion from T cells (Fig. 5A) and increased CD8+ T cell numbers (Fig. 5B) in the co-culture system. There were no significant changes in T cell activity in cultures containing macrophages differentiated in the presence of the negative control antibody.

Anti-LILRB2 blocking antibody was added in combination with anti-PD-1 antibody to PBMC co-cultures combining cells from two allogeneic donors. Enhancement of T cell activation, evidenced by increased IFNγ, was found in PBMC co-cultures treated with the combination of anti-LILRB2 and anti-PD-1 antibodies, while T cell activation was not significant in anti-PD-1 treated PBMC co-cultures (Fig. 5C).

Taken together, treatment with blocking anti-LILRB2 antibody augments the stimulation of T cells in autologous and allogenic co-cultures by promoting the activation and T cell stimulating capabilities of LILRB2 expressing monocytes and macrophages.

In support of this notion, JTX-8064 treated monocytes from healthy donors showed significant changes in gene expression using a NanoString panel (Fig. 5D). Furthermore, when these monocytes were differentiated in the presence of blocking anti-LILRB2 antibody into either HMDM or human monocyte-derived dendritic cells (HMDDCs) significant protein expression changes were detected by flow cytometry, including decrease in CD163 expression on macrophages and DCs, significant upregulation of CD86 expression on DCs and significant downregulation of DC-Sign expression (Fig. 5E and 5F). Gene expression measurements revealed significant changes in monocytes differentiated into DCs or macrophages in the presence of anti-LILRB2 antibody, when compared to isotype control-treated cells (Supplemental Fig. 8). These changes indicated that LILRB2 plays a significant role in preventing the emergence of immunostimulatory macrophages and DCs. Based on these findings we hypothesize that anti-LILRB2 antibody treatment of cancer patients will have the capability to change the phenotype of monocytes that are recruited into the tumor environment and these monocytes will be differentiated into more immunostimulatory macrophages and DCs cells better adept at activating T cells.

**JTX-8064 induces immunostimulatory polarization of macrophages and T cell activation in a subset of *ex vivo* cultured human tumor samples**

We evaluated the effects of JTX-8064 in a human tumor *ex vivo* histoculture, which recapitulates an intact tumor microenvironment, without cells being dissociated. Surgically excised tumor tissue is sectioned into slices that are incubated *ex vivo* in the presence or absence of test molecules. Both pre- and post-treatment samples are collected and analyzed for changes in gene expression to measure drug response. We studied the effect of JTX-8064 monotherapy treatment on pharmacodynamic gene signatures in 120 histoculture samples isolated from various solid tumors. The macrophage polarization score was significantly increased in 8 out of 50 (16%) renal cell cancer, 11 out of 28 lung cancer (39%) and 4 out of 42 head and neck tumor samples (10%) following treatment with JTX-8064 (Fig. 6A). A response threshold was determined as described in the Materials and Methods section. Patient samples above the threshold post-treatment are labeled in red.

To understand how responders can be distinguished from non-responders, both groups were characterized by gene expression and compared to each other. Pre-treatment histoculture samples were evaluated for gene expression changes that may be predictive of pharmacodynamic (PD) response post-treatment of JTX-8064 in monotherapy, as measured by macrophage polarization scores (Fig. 6B). Pathway-related genes that were predictive of macrophage polarization response to JTX-8064 after FDR correction included: HLA-A, HLA-B, HLA-C, and LILRB2. LILRB2 displayed the greatest difference in expression between responders and non-responders of all genes tested using NanoString and qPCR, making it the best predictor of macrophage polarization gene signature induction by JTX-8064 in the *ex vivo* histoculture system. Supplementary Fig. 9 shows that LILRB2 has high sensitivity and specificity as a predictive biomarker of macrophage polarization response, with the area under the receiver operating characteristic (ROC) curve equal to 0.70. LILRB2 levels are higher in pharmacodynamic responders vs. non-responders in histoculture (Fig. 6C).

We analyzed our histoculture results from anti-PD-1 (pembrolizumab) treated samples (Supplementary Figure 10A). Out of 64 anti-PD-1 treated samples, 10 showed PD response as measured using the IFNγ signature. Based on on-treatment tumor biopsies from cancer patients, it is appreciated that clinical responders to anti-PD(L)1 display tumor warming in response to these drugs. Additionally, we observed that in histoculture, an unweighted version of an 18 gene signature that has been associated with clinical response to anti-PD-1 (Ayers et al, JCI, 2017) was also associated with response to anti-PD-1 (Supplemental Figure 10B).

In MLR systems, JTX-8064 increases the activation of T cells by anti-PD-1 (Fig. 4H and Fig. 5C). We, therefore, tested the combination of JTX-8064 and pembrolizumab (anti-PD-1) within the more complex histoculture system, to test if a similar potentiation of anti-PD1 pharmacodynamic response was observed in the TME. Samples from 62 tumors were evaluated

for IFNγ PD signature upon JTX-8064 monotherapy and in combination with anti-PD-1. A response threshold was determined as described in the Materials and Methods. In a subset of 8 tumor samples, induction of IFNγ PD signature by JTX-8064 in combination with anti-PD-1 antibody was higher compared to pembrolizumab alone, converting non-responder tumors to responders (Fig. 6D). In Figure 6E, 4 patient samples are shown in which IFNγ PD signature was induced by JTX-8064 or anti-PD-1, but there was no increased effect observed in the combination of the two.

As measured by significant increases of the IFNγ PD signature, out of 29 kidney tumor samples treated, 3 responded to JTX-8064, 2 responded to anti-PD-1 antibody, and 3 responded to the combination treatment by the IFNγ PD signature. Out of 11 lung tumor samples treated, 2 responded to JTX-8064, 2 responded to anti-PD-1 antibody, and 2 responded to the combination treatment. Out of 22 head and neck tumor samples treated, 3 responded to JTX-8064, 5 responded to anti-PD-1 antibody, and 7 responded to the combination treatment by the IFNγ PD signature.

To further understand the translatability of our histoculture analyses, we re-analyzed 3 datasets from previously published work. In RNAseq datasets interrogating pre-treatment biopsies in 3 tumor types (urothelial, melanoma, and gastric cancer) prior to treatment with either anti-PD-1 or anti-PD-L1 therapy, we identified an association between LILRB2 expression and an IFNγ signature and patient's response to treatment. Non-responders (stable disease and progressive disease) compared to responders (complete response, partial response) had significantly higher intra-tumoral LILRB2 levels relative to the IFNγ signature ($p$ <0.01) suggesting LILRB2 may be involved in primary resistance to checkpoint blockade (Fig 6F). Similarly, histoculture samples that had a pharmacodynamic response to anti-PD-1 treatment at baseline expressed lower levels of LILRB2 surrogate gene signature in a ratio with IFNγ signature (Fig. 6G).

Collectively, these histoculture data demonstrate that JTX-8064 can drive the polarization of macrophages and can indirectly activate T cells within the TME and may help to improve response to PD-1 inhibitors within an explant tumor histoculture system.

## DISCUSSION

Our study demonstrates that blockade of cell surface receptor LILRB2 by the monoclonal antibody JTX-8064 has the potential to activate multiple cell types within myeloid compartment within the TME. Circulating LILRB2+ monocytes, differentiated into HMDMs or DCs in the presence of anti-LILRB2 antibody, develop into macrophages and DCs with an immunostimulatory phenotype. This is evidenced by decreased expression of the immunosuppressive marker CD163 on macrophages and increased expression of the activation marker CD86 on DCs as well as increased macrophage-dependent T cell activation following treatment with anti-LILRB2 antibody. Furthermore, macrophages within tumors can be activated by JTX-8064 to an inflammatory phenotype as shown in *ex vivo* histoculture and *in*

*vitro* assays. Based on these findings we propose JTX-8064 modifies the tumor microenvironment to become immune stimulatory in at least two ways: first by enhancing monocyte activation as they differentiate into tumor-associated macrophages and DCs, and second by a direct pro-inflammatory polarization effect on tumor-associated macrophages. Consequently, alteration of the myeloid compartment by JTX-8064 has to the potential to increase T cell proliferation and effector cytokine secretion.

JTX-8064 enhances T cell stimulation in combination with anti-PD-1 antibody treatment in histoculture and in PBMC allogeneic reactions. At the same time, activation of T cells indirectly by JTX-8064 can be observed without the addition of T cell-centric IO agents such as anti-PD-1 antibody in macrophage co-culture assays and in a subset of samples in the histoculture system. These data suggest that JTX-8064 can act as a bridge between the innate and adaptive immune systems, by directly reversing the T cell suppressive capability of macrophages and DCs resident to the tumor or recruited into the TME.

LILRB2 is also highly expressed by monocytes and neutrophils in peripheral blood in both cancer patients and healthy volunteers. Intermediate monocytes are a subset of monocytes found in the peripheral blood expressing CD14 and high levels of CD16. While the function of intermediate monocytes in cancer is not entirely known, reports indicate that high levels of these monocytes in cancer patient blood is indicative of poor prognosis[27] and associated with high tumor burden[28]. We have found that intermediate monocytes express high level of LILRB2 in healthy donors as well as in cancer patients. Expression of LILRB2 in circulating intermediate monocytes may be indicative of an immunosuppressive phenotype of this cell type and requires further investigation.

LILRB2 expressing TAMs play a key role in the resistance mechanisms to PD-1 inhibitor therapies in a variety of tumor types, suppressing T cell responses in the TME. TAMs can suppress T cell activation in multiple ways. For example, TAMs consume metabolites that are essential for robust T cell activation. This was first shown in a mouse model expressing arginase 1 (ARG1), which can actively suppress the proliferation of T cells[29]. ARG1 expressed in myeloid cells metabolizes L-arginine, a critical amino acid required for robust T cell activation[30]. Secreted factors by the immunosuppressive M2-like macrophages can also directly inhibit T cell activation. For example, macrophage-derived granulin has been shown to inhibit T cells and correspond to PD-1 inhibitor resistance in pancreatic cancer[31]. Exosomes secreted by tumor-resident macrophages contain miRNA that shift the balance towards regulatory T cells in the tumor T cell compartment in ovarian cancer[32]. Indoleamine 2,4-Dioxygenase (IDO) produced by macrophages has been shown to down-regulate T cell responses[33] Immunoinhibitory cytokine production (e.g., IL-10, TGFβ and PGE2) by TAMs can also suppress T cell activation. Importantly, these immunosuppressive macrophage phenotypes are established and sustained by signaling events through key macrophage immune checkpoint receptors, such as LILRB2. The binding of LILRB2 to MHC-I molecules has been shown to drive these impactful signaling cascades triggering immunoinhibitory differentiation[17,34].

Taken together, our data demonstrate that JTX-8064 is an inhibitor of the macrophage checkpoint receptor LILRB2 and can polarize macrophage and DC cells toward a more immunostimulatory phenotype with T cell activation potential. The evidence gathered from *in vitro* and *ex vivo* responses to JTX-8064 and evaluation of predictive gene signatures in clinical response data supports the development of JTX-8064 in combination with PD-1(L1) inhibitors in multiple tumor types, with the potential to use predictive biomarkers to guide clinical development. Recent phase I data on MK-4830, another anti-LILRB2 blocking antibody, showed clinical benefit in combination with pembrolizumab in patients with advanced solid tumors, including those who had previously received a PD-1 inhibitor[35]. The activity of JTX-8064 in cell culture and ex vivo human tumors combined with the observation that patients with high LILRB2 expression relative to an IFNγ gene signature are less likely to respond to anti-PD(L)-1 therapy provides a rationale that JTX-8064 may be able to overcome anti-PD-1 primary resistance mechanisms. JTX-8064 is currently being developed as monotherapy and in combination with PD-1 inhibitor therapy in a range of solid tumors (NCT04669899).

**Acknowledgement**

**The authors would like to acknowledge all our Jounce Therapeutics colleagues who have contributed to this work. Especially, Dr. Ed Stack who poured himself into this work, a brilliant pathologist, scientist, and colleague. Rest in peace dear friend. We extend special thanks to Dr. Haley Laken for her thoughtful review and feedback on this manuscript.**

**REFERENCES**

1. Mantovani, A., S. Sozzani, M. Locati, P. Allavena, and A. Sica. Macrophage polarization: tumor-associated macrophages as a paradigm for polarized M2 mononuclear phagocytes, *Trends Immunol*, **2002**; 23: 549-55.
2. Ma, C., H. Horlad, K. Ohnishi, T. Nakagawa, S. Yamada, S. Kitada, *et al.* CD163-positive cancer cells are potentially associated with high malignant potential in clear cell renal cell carcinoma, *Med Mol Morphol*, **2018**; 51: 13-20.
3. Nakayama, T., K. Saito, J. Kumagai, Y. Nakajima, T. Kijima, S. Yoshida, *et al.* Higher Serum C-reactive Protein Level Represents the Immunosuppressive Tumor Microenvironment in Patients With Clear Cell Renal Cell Carcinoma, *Clin Genitourin Cancer*, **2018**; 16: e1151-e58.

4. Komohara, Y., H. Hasita, K. Ohnishi, Y. Fujiwara, S. Suzu, M. Eto, *et al.* Macrophage infiltration and its prognostic relevance in clear cell renal cell carcinoma, *Cancer Sci*, **2011**; 102: 1424-31.
5. Hensler, M., L. Kasikova, K. Fiser, J. Rakova, P. Skapa, J. Laco, *et al.* M2-like macrophages dictate clinically relevant immunosuppression in metastatic ovarian cancer, *J Immunother Cancer*, **2020**; 8.
6. Yuan, X., J. Zhang, D. Li, Y. Mao, F. Mo, W. Du, *et al*. Prognostic significance of tumor-associated macrophages in ovarian cancer: A meta-analysis, *Gynecol Oncol*, **2017**; 147: 181-87.
7. Balermpas, P., F. Rodel, R. Liberz, J. Oppermann, J. Wagenblast, S. Ghanaati, *et al.* Head and neck cancer relapse after chemoradiotherapy correlates with CD163+ macrophages in primary tumour and CD11b+ myeloid cells in recurrences, *Br J Cancer*, **2014**; 111: 1509-18.
8. Troiano, G., V. C. A. Caponio, I. Adipietro, M. Tepedino, R. Santoro, L. Laino, *et al.* Prognostic significance of CD68(+) and CD163(+) tumor associated macrophages in head and neck squamous cell carcinoma: A systematic review and meta-analysis, *Oral Oncol*, **2019**; 93: 66-75.
9. Willcox, B. E., L. M. Thomas, T. L. Chapman, A. P. Heikema, A. P. West, Jr., and P. J. Bjorkman. Crystal structure of LIR-2 (ILT4) at 1.8 A: differences from LIR-1 (ILT2) in regions implicated in the binding of the Human Cytomegalovirus class I MHC homolog UL18, *BMC Struct Biol*, **2002**; 2: 6.
10. Shiroishi, M., K. Kuroki, L. Rasubala, K. Tsumoto, I. Kumagai, E. Kurimoto, *et al.* Structural basis for recognition of the nonclassical MHC molecule HLA-G by the leukocyte Ig-like receptor B2 (LILRB2/LIR2/ILT4/CD85d), *Proc Natl Acad Sci U S A*, **2006**; 103: 16412-7.
11. Wang, Q., H. Song, H. Cheng, J. Qi, G. Nam, S. Tan, *et al.* Structures of the four Ig-like domain LILRB2 and the four-domain LILRB1 and HLA-G1 complex, *Cell Mol Immunol*, **2020**; 17: 966-75.
12. Burshtyn, D. N., and C. Morcos. The Expanding Spectrum of Ligands for Leukocyte Ig-like Receptors, *J Immunol*, **2016**; 196: 947-55.
13. Carosella, E. D., P. Moreau, J. Lemaoult, and N. Rouas-Freiss. HLA-G: from biology to clinical benefits, *Trends Immunol*, **2008**; 29: 125-32.
14. Huang, J., P. Burke, Y. Yang, K. Seiss, J. Beamon, T. Cung, m *et al.* Soluble HLA-G inhibits myeloid dendritic cell function in HIV-1 infection by interacting with leukocyte immunoglobulin-like receptor B2, *J Virol*, **2010**; 84: 10784-91.
15. Bashirova, A. A., E. Martin-Gayo, D. C. Jones, Y. Qi, R. Apps, X. Gao, *et al.* LILRB2 interaction with HLA class I correlates with control of HIV-1 infection, *PLoS Genet*, **2014;** 10: e1004196.
16. Krijgsman, D., J. Roelands, W. Hendrickx, D. Bedognetti, and P. J. K. Kuppen. HLA-G: A New Immune Checkpoint in Cancer?, **2020**; *Int J Mol Sci*, 21.
17. Chen, H. M., W. van der Touw, Y. S. Wang, K. Kang, S. Mai, J. Zhang, *et al.* Blocking immunoinhibitory receptor LILRB2 reprograms tumor-associated myeloid cells and promotes antitumor immunity, *J Clin Invest*, **2018**; 128: 5647-62.

18. Martinez, F. O., S. Gordon, M. Locati, and A. Mantovani. Transcriptional profiling of the human monocyte-to-macrophage differentiation and polarization: new molecules and patterns of gene expression, *J Immunol*, **2006**; 177: 7303-11
19. Cillo, A. R., C. H. L. Kurten, T. Tabib, Z. Qi, S. Onkar, T. Wang, *et al.* Immune Landscape of Viral- and Carcinogen-Driven Head and Neck Cancer, *Immunity*, **2020**; 52: 183-99 e9.
20. Sade-Feldman, M., K. Yizhak, S. L. Bjorgaard, J. P. Ray, C. G. de Boer, R. W. Jenkins, *et al.* Defining T Cell States Associated with Response to Checkpoint Immunotherapy in Melanoma, *Cell*, **2018**; 175: 998-1013 e20.
21. Qian, J., S. Olbrecht, B. Boeckx, H. Vos, D. Laoui, E. Etlioglu, *et al.* A pan-cancer blueprint of the heterogeneous tumor microenvironment revealed by single-cell profiling, *Cell Res*, **2020**; 30: 745-62.
22. Puram, S. V., I. Tirosh, A. S. Parikh, A. P. Patel, K. Yizhak, S. Gillespie, *et al.* Single-Cell Transcriptomic Analysis of Primary and Metastatic Tumor Ecosystems in Head and Neck Cancer, *Cell*, **2017**; 171: 1611-24 e24.
23. Lambrechts, D., E. Wauters, B. Boeckx, S. Aibar, D. Nittner, O. Burton, *et al.* Phenotype molding of stromal cells in the lung tumor microenvironment, *Nat Med*, **2018**; 24: 1277-89.
24. Karaayvaz, M., S. Cristea, S. M. Gillespie, A. P. Patel, R. Mylvaganam, C. C. Luo, *et al.*. Unravelling subclonal heterogeneity and aggressive disease states in TNBC through single-cell RNA-seq, **2018**; *Nat Commun*, 9: 3588
25. Tirosh, I., B. Izar, S. M. Prakadan, M. H. Wadsworth, 2nd, D. Treacy, J. J. Trombetta, A. *et al.* Dissecting the multicellular ecosystem of metastatic melanoma by single-cell RNA-seq, *Science*, **2016**; 352: 189-96.
26. Jayasingam, S. D., M. Citartan, T. H. Thang, A. A. Mat Zin, K. C. Ang, and E. S. Ch'ng. Evaluating the Polarization of Tumor-Associated Macrophages Into M1 and M2 Phenotypes in Human Cancer Tissue: Technicalities and Challenges in Routine Clinical Practice, *Front Oncol*, **2019**; 9: 1512.
27. Prat, M., A. Le Naour, K. Coulson, F. Lemee, H. Leray, G. Jacquemin, *et al.* Circulating CD14(high) CD16(low) intermediate blood monocytes as a biomarker of ascites immune status and ovarian cancer progression, *J Immunother Cancer*, **2020**; 8.
28. Schauer, D., P. Starlinger, C. Reiter, N. Jahn, P. Zajc, E. Buchberger, *et al.* Intermediate monocytes but not TIE2-expressing monocytes are a sensitive diagnostic indicator for colorectal cancer, *PLoS One*, **2012**; 7: e44450.
29. Bronte, V., P. Serafini, C. De Santo, I. Marigo, V. Tosello, A. Mazzoni, *et al.* IL-4-induced arginase 1 suppresses alloreactive T cells in tumor-bearing mice, *J Immunol*, **2003;** 170: 270-8.
30. Grzywa, T. M., A. Sosnowska, P. Matryba, Z. Rydzynska, M. Jasinski, D. Nowis, *et al.* Myeloid Cell-Derived Arginase in Cancer Immune Response, *Front Immunol*, **2020;** 11: 938.
31. Quaranta, V., C. Rainer, S. R. Nielsen, M. L. Raymant, M. S. Ahmed, D. D. Engle, *et al.* Macrophage-Derived Granulin Drives Resistance to Immune Checkpoint Inhibition in Metastatic Pancreatic Cancer, *Cancer Res*, **2018**; 78: 4253-69.

32. Zhou, J., X. Li, X. Wu, T. Zhang, Q. Zhu, X. Wang, *et al.* Exosomes Released from Tumor-Associated Macrophages Transfer miRNAs That Induce a Treg/Th17 Cell Imbalance in Epithelial Ovarian Cancer, *Cancer Immunol Res*, **2018**; 6: 1578-92.

33. Zhao, Q., Kuang, D-M., Wu, Y., Xiao, X., Li, X-F., Li, T-J., *et al.* Activated CD69+ T cells foster immune priviledge by regulating IDO expression in tumor-associated macrophages, *J Immunol*, **2012**; 188(3):1117-24.
34. Deng, M., H. Chen, X. Liu, R. Huang, Y. He, B. Yoo, *et al.* Leukocyte immunoglobulin-like receptor subfamily B: therapeutic targets in cancer, *Antib Ther*, **2021**; 4: 16-33.
35. Siu, L., D. Wang, J. Hilton, R. Geva, D. Rasco, R. Perets, *et al.* First-in-Class Anti-immunolobulin-like Transcript 4 Myeloid Specifc Antibody MK-4830 Abrogates a PD-1 Resistance Mechanism in Patients with Advanced Solid Tumors, *Clinical Cancer Research* **2022**; 28 (1): 57-70.
36. Kim, S.T., R. Cristescu, A.J. Bass, K-M Kim, J.I. Oldegaard, K. Kim, *et al*. Comprehensive molecular characterization of clinical responses to PD-1 inhibition in metastatic gastric cancer, *Nature Medicine*, **2018**; 24, 1339-1458.
37. Mariathasan, S., S. J. Turley, D. Nickles, A. Castiglioni, K. Yuen, Y. Wang *et al*. TGFβ attenuatrs tumour response to PD-L1 blockade by contributing to exclusion of T cells, *Nature,* **2018;** 554, 544-548.
38. Riaz, N., J.J. Havel, V. Makarov, A. Desrichard, W.J. Urba, J.S. Sims, *et al.* Tumor and Microenviornemtn Evolution during Immunotherapy with Nivolumab, *Cell*, **2017**; 171(4):934-949.

**Figure Legends**

**Figure 1: LILRB2 is primarily expressed on myeloid cells in the tumor microenvironment.**

scRNAseq analysis from published data sets. Tumor associated macrophage signature, LILRB2 and cell type specific signatures from tumor immune single cell transcriptomic data from (A) head and neck (Cillo et al. 2020), (B) melanoma (Sade-Feldman et al. 2018), (C) CRC, NSCLC, breast and ovarian (Qian et al. 2020) tumors.

**Figure 2: LILRB2 is highly expressed in circulating immune cells in healthy donors and cancer patients.**

(A, B) Quantification of LILRB2 from healthy blood, cancer patient blood and TILs by flow cytometry in various immune cells. Assuming monovalent antibody-to-surface receptor binding, the values reported are the average number of LILRB2 receptors per cell for monocytes, neutrophils, B cells and T cells. One way ANOVA multiple comparison test *p<.05, ***p<.001, ****p<.0001. (C) LILRB2 copy number per cell (D) in 5 healthy donor and 29 cancer patient blood samples (5 ovarian, 4 head and neck, 10 NSCLC, 10 renal cancer patients), means and +/- SEM. One way ANOVA multiple comparison test *p<.05, ***p<.001, ****p<.0001.

**Figure 3: JTX-8064 specifically binds LILRB2 and blocks HLA-A and HLA-G ligand binding.**

(A) JTX-8064 (10 μg/mL) binds specifically to LILRB2 overexpressing CHO-S cells and not parental CHO-S cells or CHO-S cells overexpressing other LILRB or LILRA family members as measured by FACS. Cell surface expression of LILRB/LILRA was confirmed by staining all cell lines with polyclonal anti-LILR antibody (AF2078). (B) JTX-8064 was captured on the SPR chip surface followed by injection of LILRB2 ECD His-tag protein in 2.5-fold serial dilutions with a top concentration of 60 nM. 1:1 Langmuir fit is shown in black. (C) JTX-8064 binding to monocytes and Neutrophils full dose response curves as measured by fold over isotype. JTX-8064 potently blocks (D) HLA-G and (E) HLA-A2 tetramers from binding to human monocyte-derived macrophages and (F) HLA-G tetramer on CHO cells overexpressing LILRB2. JTX-8064 or control antibodies were added in dose titration to HMDMs or OCLs along with HLA-G or HLA-A2 tetramers labeled with an APC conjugate. Maximal tetramer binding is the FACS-determined MFI of HMDMs plus tetramer in the absence of antibodies.

**Figure 4: JTX-8064 enhances pro-inflammatory activation of macrophages and down-regulates key immunoinhibitory signaling.**

HMDMs were stimulated with LPS and JTX-8064 for 24h at which time supernatants were assayed for (A) TNFα or (B) IL-10. (C) HMDMs were cultured with a LILRB2-specific blocking antibody (RCM15) or isotype control in the absence of any additional stimulation. After 24 hours, RNA was harvested for NanoString analysis. (D) Specific genes that are identified as M1-like or M2-like displayed as fold change over isotype by anti-LILRB2 antibody. Protein level expression on HMDMs of (E) CD163 and (F) CD14 by MFI measured by flow cytometry post-treatment for 2 days of JTX-8064 treatment. (G) HMDMs were lysed after 24 hours of LPS and anti-LILRB2 treatment and pSTAT3 was measured by ELISA. Data displayed as means of 4-6 healthy donors with +/- SEM and significance by Student's t-test *<.05, **<.01. (H) Levels of

IFNγ detected in the allogenic MLR supernatants after a 5-day incubation of total PBMCs from 2 donors. Values are normalized to the level of IFNγ with hIgG4 isotype control treatment from each donor pair. Each point represents the mean of triplicate cultures from each donor pair is displayed with a total of 22 unique donor pairs. All antibodies were treated at 10 mg/ml at day 0. An ordinary one-way ANOVA multiple comparison test was performed * represents a p value < 0.05 from an ordinary one-way ANOVA ** represents a p value < 0.01. Error bars represent standard error of the mean.

**Figure 5: Anti-LILRB2 alters monocyte differentiation to macrophage and DCs, driving a more T cell activating phenotype.**

*In vitro* activation of T cells by macrophages differentiated in the presence of JTX-8064. Peripheral monocytes isolated from healthy donors and differentiated into macrophages in the presence of JTX-8064 or a control IgG4 antibody. Autologous T cells and anti-CD3 antibody are added to a co-culture for 3 days with the macrophages (at a 1:8 ratio of T cells:macrophages). After 3 days, (A) IFNγ and (B) the number of CD8 T cells were significantly upregulated in co-cultures in which macrophages were differentiated in the presence of JTX-8064 compared to the control antibody (4 donors, *** p=.0007 two-way ANOVA; 1 representative donor, 3 biological replicates, ** p=.0012 two-way ANOVA) (C) PMBC/PBMC allogenic mixed reactions. Each point represents the mean of triplicate cultures from each donor pair is displayed with a total of 10 unique donor pairs. All antibodies were treated at 10 mg/ml at day 0. An ordinary one-way ANOVA multiple comparison test was performed * represents a p value < 0.05 from an ordinary one-way ANOVA ** represents a p value < 0.01. Error bars represent standard error of the mean. (D) Monocytes were isolated from whole blood PBMCS from 6 healthy donors and treated with JTX-8064 or isotype control for 24h. NanoString analysis was performed on isolated RNA. Volcano plot of fold change over isotype and p-value significance. (E) Monocytes differentiated in the presence of JTX-8064 or isotype control for 7 days with GM-CSF and IL-4 (F) or M-CSF. CD86, DC-SIGN, and CD163 MFI measured by flow cytometry. Mean of 6 donors +/- SEM. Student's t-test was performed, *p<.05, **p<.001, ***p<.001, ****p<.0001.

**Figure 6: JTX-8064 induces inflammatory polarization and T cell activation gene expression signatures in a subset of unselected *ex vivo* cultured human tumor samples with relevant gene signatures predictive of response to both JTX-8064 and anti-PD-1 in ex vivo system identified.**

A strict noise threshold was set as described in materials and methods for each signature score. Each circle represents an individual tumor sample. (A). Those samples scoring positive (>95$^{th}$ percentile of noise distribution) are above the dotted line in red and are deemed to have

induced the indicated gene signature in response to JTX-8064 treatment in monotherapy. Non-responding samples are shown in blue for the macrophage polarization signature (B) Volcano plot displaying p value significance by baseline mRNA level fold over differences between responders and non-responder tumors for macrophage polarization signature response in *ex vivo* culture system. LILRB2 was measured using qPCR, the expression of all other genes was measured using NanoString. Nominal p values are shown (C) LILRB2 expression in tumor samples prior to treatment with JTX-8064, samples that responded with increases in the macrophage polarization score are labeled "R" in red and samples that did not respond are labeled "NR" in blue (D) . In 12 out of 62 *ex vivo* treated human tumor samples, the combination of JTX-8064 plus anti-PD-1 antibody showed a significant IFNγ signature response. In 8 of the 12, the combination resulted an overall enhancement in the magnitude of the IFNγ signature score compared to when the same tumor was treated with anti-PD-1 antibody as a single agent. (E) In 4 of the 12, no significant combination benefit was observed in patient samples that responded to monotherapy JTX-8064 or anti-PD-1. To better understand predictive RNA biomarkers to anti-PD-(L)1 treatment outcome, analysis was performed on histoculture (F) on published studies (G) that evaluated pre-treatment tumor biopsies with response to anti-PD-(L)1 treatment. Using a ratio of LILRB2 surrogate signature to IFNɣ Signature score, we observed non-responders (PD, SD) to anti-PD-(L)1 had significantly higher LILRB2 relative to IFNɣ that responders (CR, PR) in three studies.[36,37,38]

# FIGURE 1

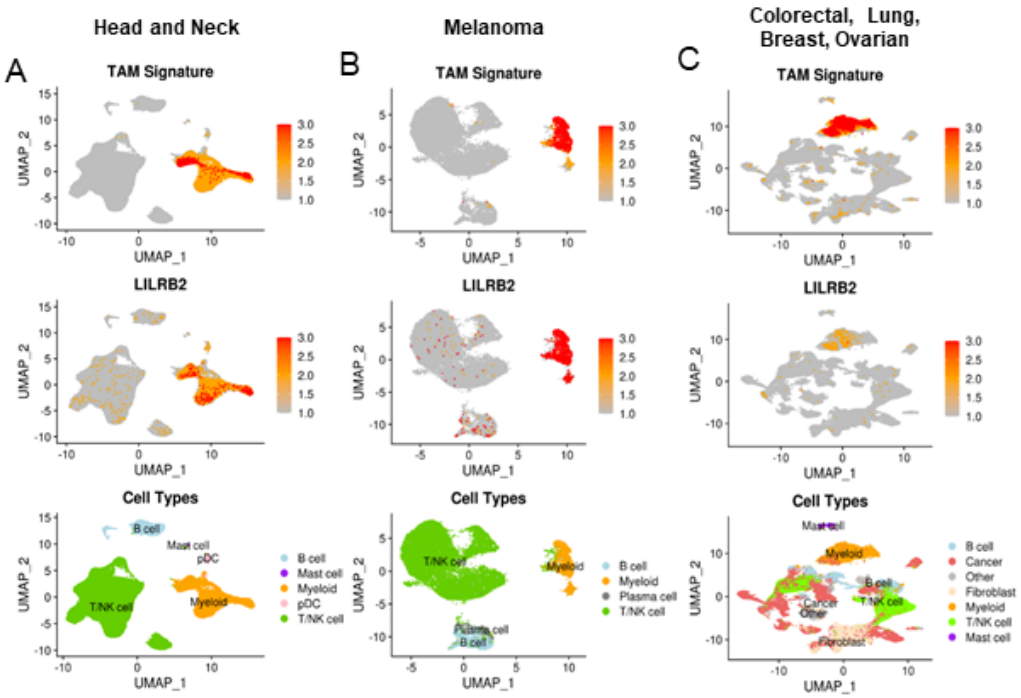

FIGURE 2

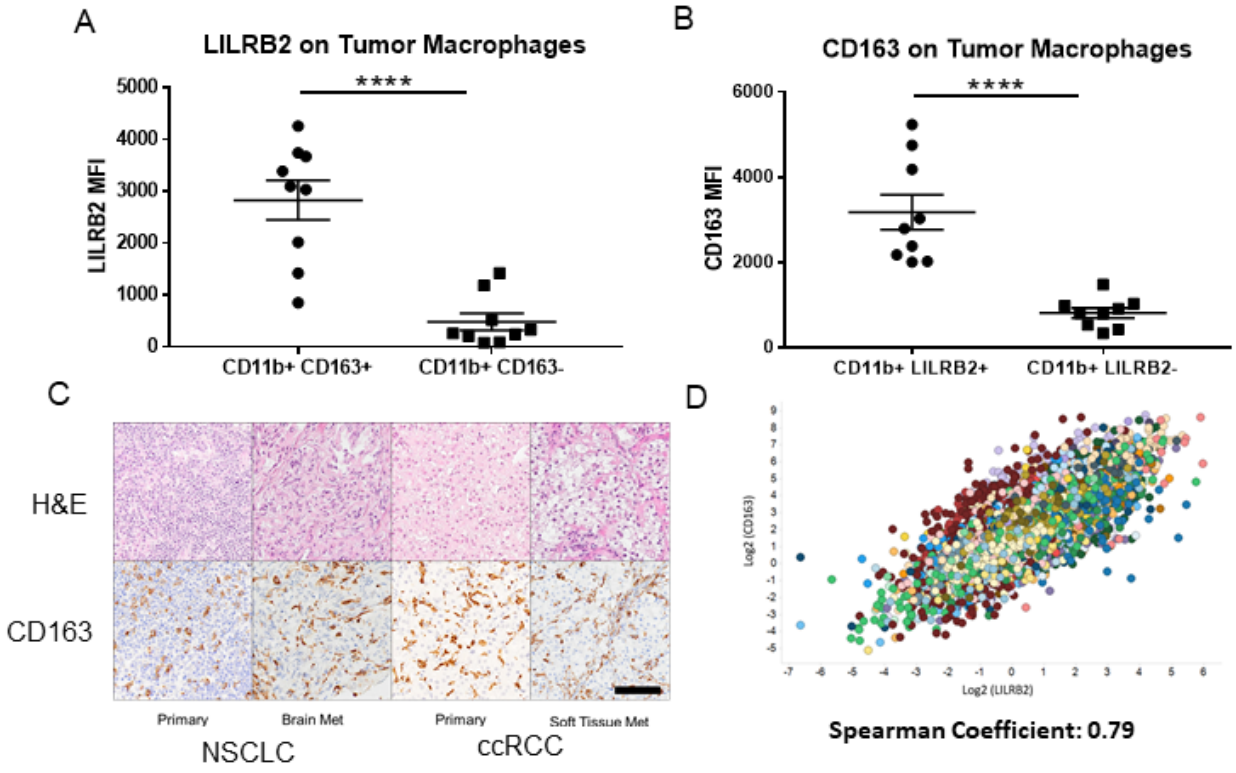

# FIGURE 3

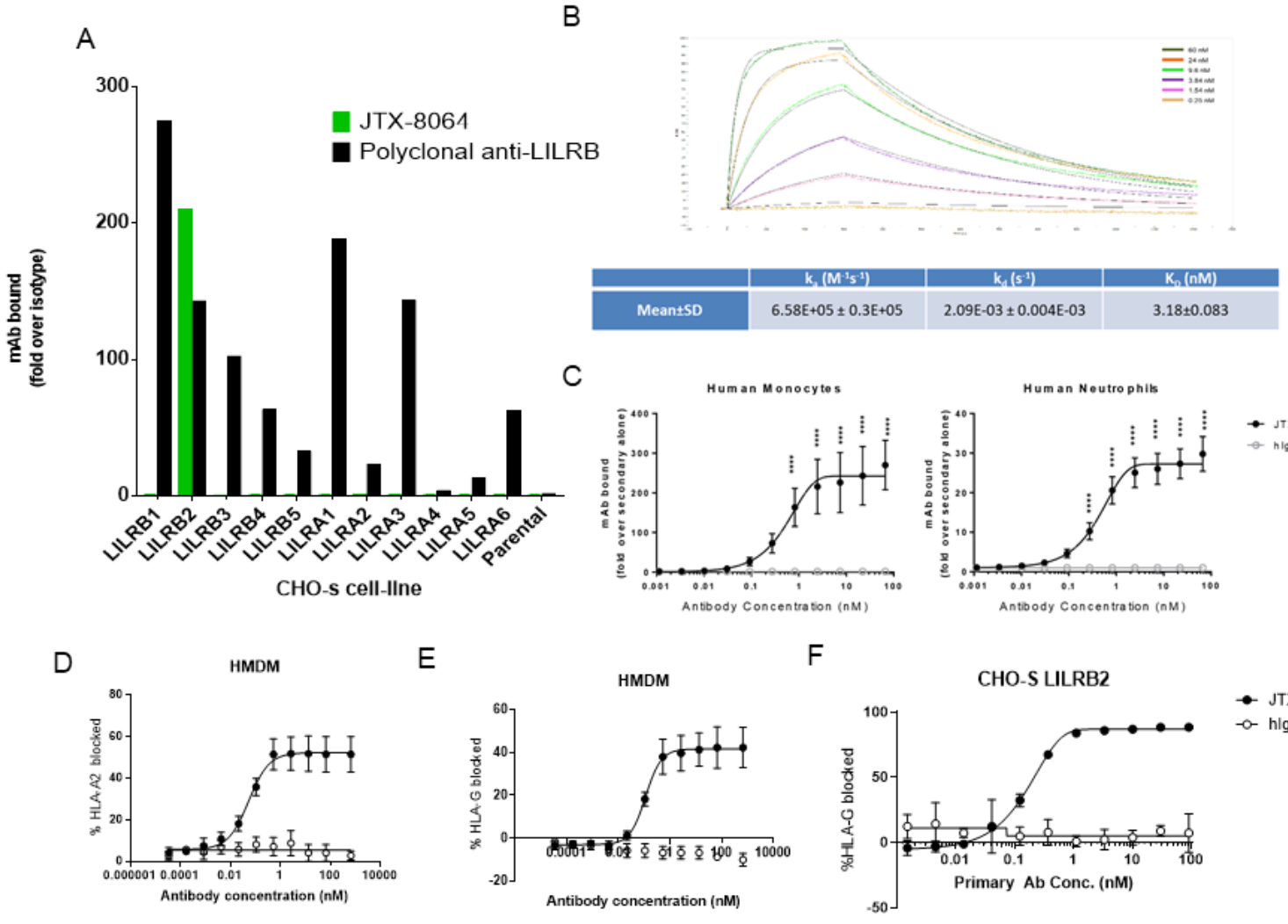


| | $k_a$ ($M^{-1}s^{-1}$) | $k_d$ ($s^{-1}$) | $K_D$ (nM) |
|---|---|---|---|
| Mean±SD | 6.58E+05 ± 0.3E+05 | 2.09E-03 ± 0.004E-03 | 3.18±0.083 |

# FIGURE 4

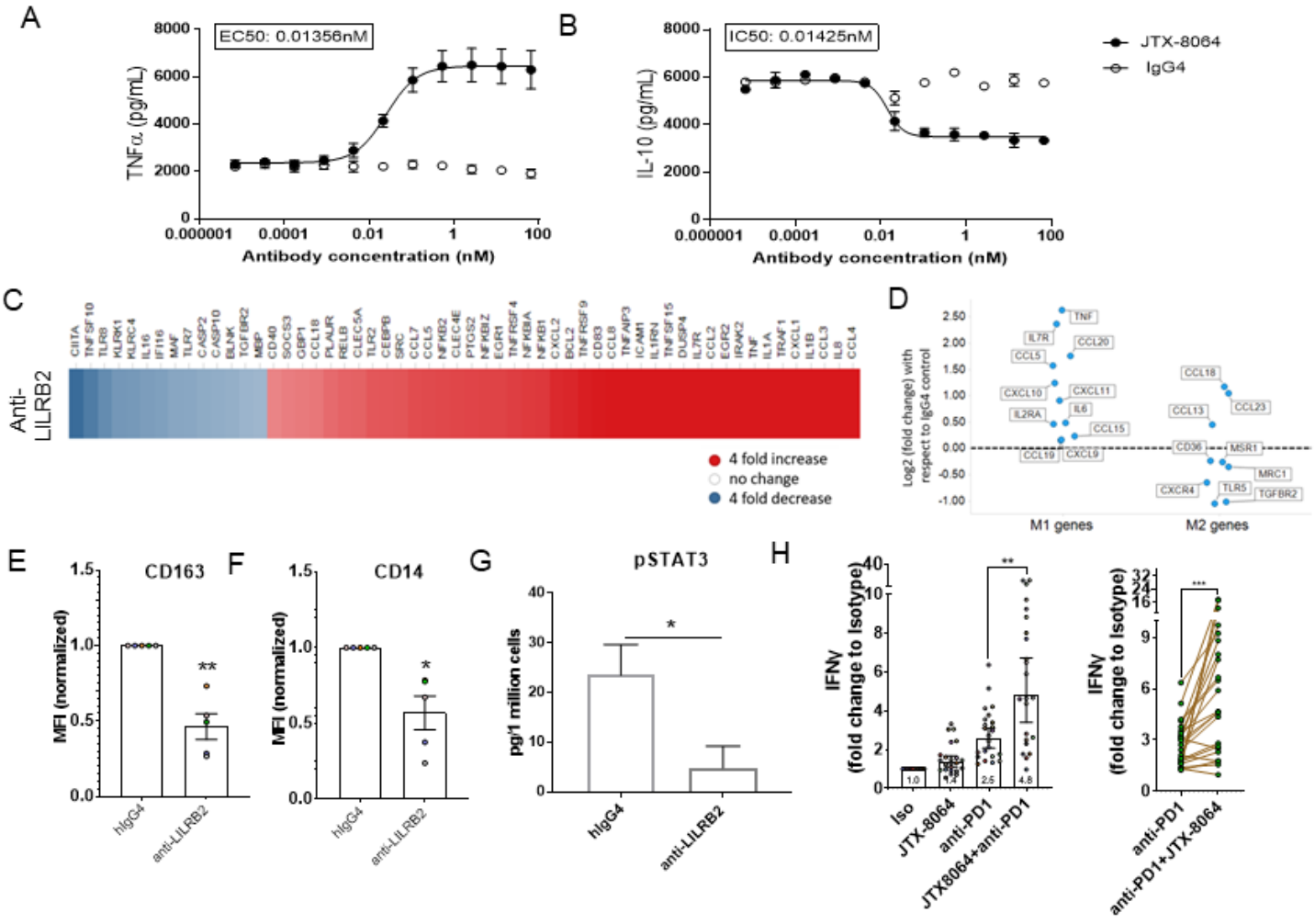

# FIGURE 5

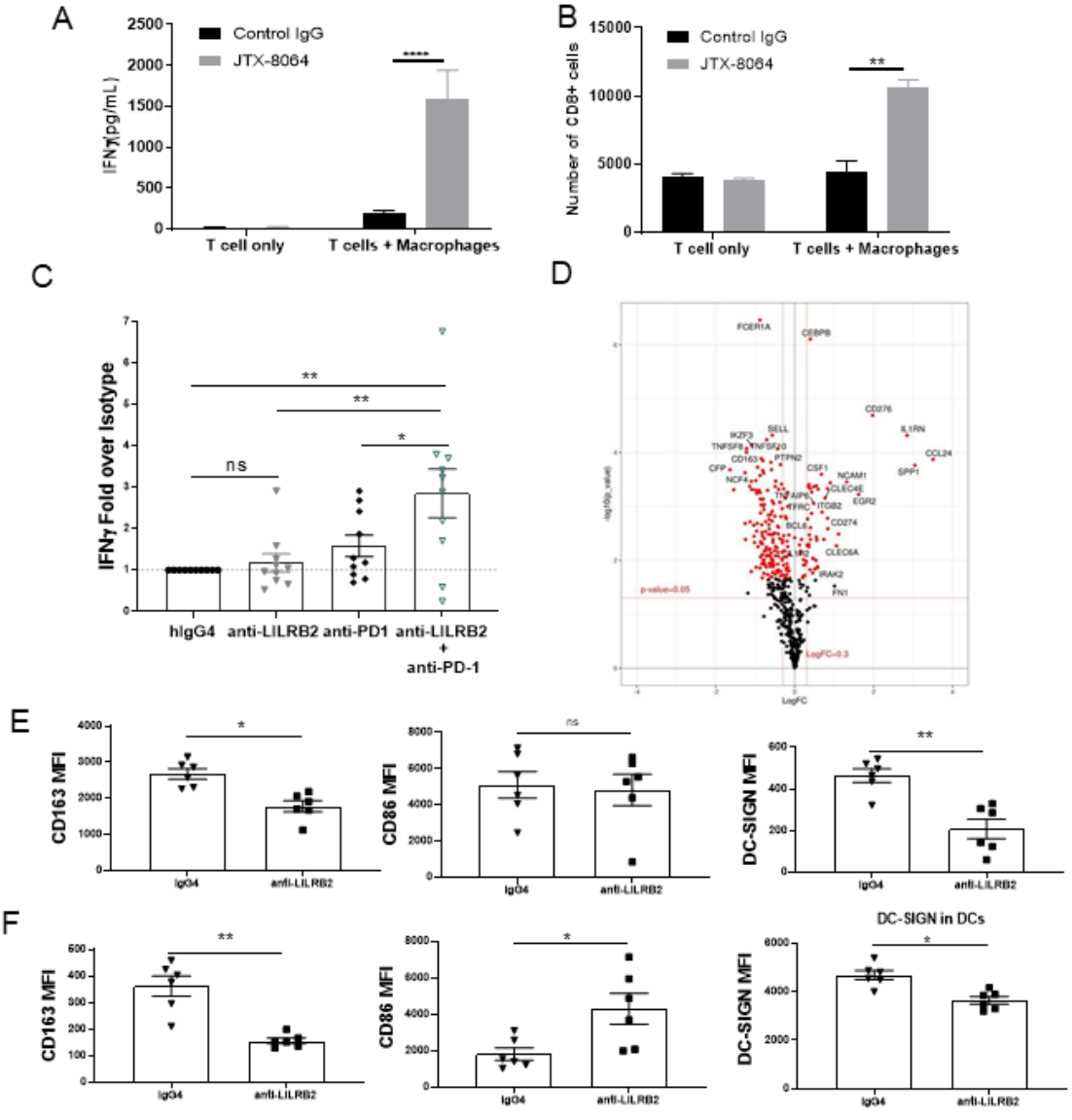

# FIGURE 6